UC Riverside
2017 Publications

Title
Distributed Signals of Opportunity Aided Inertial Navigation with Intermittent Communication

Permalink
https://escholarship.org/uc/item/1c43j1zm

Authors
Morales, J.
Kassas, Z.

Publication Date
2017-09-01

Peer reviewed

eScholarship.org Powered by the California Digital Library
University of California

Distributed Signals of Opportunity Aided Inertial Navigation with Intermittent Communication

Joshua J. Morales and Zaher M. Kassas
University of California, Riverside

BIOGRAPHIES

Joshua J. Morales is pursuing a Ph.D. from the Department of Electrical and Computer Engineering at the University of California, Riverside and a member of the Autonomous Systems Perception, Intelligence, and Navigation (ASPIN) Laboratory. He received a B.S. in Electrical Engineering with High Honors from The University of California, Riverside. In 2016 he was accorded an Honorable Mention from the National Science Foundation. His research interests include estimation, navigation, autonomous vehicles, and intelligent transportation systems.

Zaher (Zak) M. Kassas is an assistant professor at the University of California, Riverside and director of the ASPIN Laboratory. He received a B.E. in Electrical Engineering from the Lebanese American University, an M.S. in Electrical and Computer Engineering from The Ohio State University, and an M.S.E. in Aerospace Engineering and a Ph.D. in Electrical and Computer Engineering from The University of Texas at Austin. From 2004 through 2010 he was a research and development engineer with the LabVIEW Control Design and Dynamical Systems Simulation Group at National Instruments Corp. His research interests include cyber-physical systems, estimation theory, navigation, autonomous vehicles, and intelligent transportation systems.

ABSTRACT

A distributed signal of opportunity (SOP)-aided inertial navigation system (INS) framework is presented and studied for vehicles collaborating in an imperfect communication channel. The following scenario is considered. Multiple autonomous vehicles (AVs) are aiding their onboard INSs with global navigation satellite system (GNSS) signals. The AVs draw pseudorange observations from unknown SOPs in their vicinity and fuse these observations through an estimator to improve the quality of their navigation solution while simultaneously mapping the SOPs' states. While navigating, GNSS signals become unavailable, at which point the AVs continue navigating by aiding their INSs' with SOP pseudorange observations. The AVs exchange INS data, pseudorange observations, and state estimates over a lossy channel. This paper presents a distributed framework for AVs to share INS information and studies this framework by varying both the number of collaborating AVs and the probability of communication failure. Simulation and experimental results for unmanned aerial vehicles (UAVs) are presented demonstrating the performance of the distributed framework in lossy communication channels.

I. INTRODUCTION

As autonomous vehicles (AVs) move towards full autonomy, requirements on the accuracy and resiliency of the vehicle's navigation system become ever more stringent. Navigation systems on board AVs today mainly rely on integrating global navigation satellite system (GNSS) with an inertial navigation system (INS). However, in the inevitable event when GNSS signals become unavailable, uncorrected INS errors cause the AV's navigation solution to diverge. Recently, signals of opportunity (SOPs) have been considered to enable navigation whenever GNSS signals become inaccessible or untrustworthy [1–3]. AVs could exploit SOPs to correct INS errors in the absence of GNSS signals [4–6]. Collaborating AVs can share information gathered from SOPs to improve INS error corrections [7]. Unfortunately, this improvement comes with concerns inherent in communication: increased complexity, unreliable data transmission, and compromised privacy.

Navigation systems onboard AVs today typically include other sensors (e.g., cameras [**?**], lasers [8], and sonar [9]) to aid the AV's INS whenever GNSS signals become unusable. However, such aiding sensors may violate cost, size, weight, and power (C-SWAP) constraints. In contrast, SOPs (e.g., AM/FM radio [10, 11], cellular [3, 12–15], digital television [16, 17], iridium [18, 19], and Wi-Fi [20, 21]) are free to use and could alleviate the need for expensive and

Copyright © 2017 by J.J. Morales and Z.M. Kassas

Preprint of the 2017 ION GNSS+ Conference
Portland, OR, September 25–29, 2017

bulky aiding sensors. SOPs are abundant and transmitted at a wide range of frequencies and directions, making them attractive aiding sources for an INS whenever GNSS signals become unavailable. However, unlike GNSS space vehicle (SV) states, the states of SOPs, namely their position and clock error states, may not be known *a priori*, in which case they must be estimated alongside the AV's states.

This estimation problem is similar to the simultaneous localization and mapping (SLAM) problem in robotics [22]. However, in contrast to the static environmental feature map in typical SLAM problems, the SOP map is more complex since SOP clock error states are dynamic and stochastic. Recently, SLAM-type frameworks have been adopted to exploit unknown SOPs for navigation (radio SLAM) as a standalone alternative to GNSS [23, 24] and as an aiding source for an INS when GNSS signals become unavailable [5]. In [7] a centralized collaborative radio SLAM framework was presented where multiple AVs shared their inertial measurement unit (IMU) data and mutual pseudorange observations on SOPs to improve the quality of their individual INS state estimates, while building a more accurate SOP map compared to a single AV performing radio SLAM. The improvement in estimation performance is attributed to the AVs' states becoming correlated when mutual observations are fused through a central fusion center (CFC), e.g., through an extended Kalman filter (EKF) update. Therefore, when any one of the AVs processes an observation, the entire team of AVs benefit from a reduction of uncertainty in their state estimates.

Three major challenges in any collaborative navigation strategy are: (i) maintaining the cross-correlations between vehicles, (ii) large requirements on communication bandwidth, and (iii) communication link failures [**?**]. These challenges are particularly problematic for a collaborative SOP-aided INS, since each AV's uncertainty propagation is dependent on local IMU data. Therefore, propagating the cross-correlation between any two AVs requires the availability of IMU data from both AVs. Transmitting IMUS data to a CFC could be impractical since it requires (1) access to internal IMU signals from each AV, (2) a large communication bandwidth, and (3) a lossless communication channel between the AVs and the CFC. This paper's contribution is to address some of these challenges for the following scenario.

Consider multiple AVs navigating by aiding their onboard INSs with GNSS pseudoranges. The AVs draw pseudorange observations from unknown SOPs in their vicinity and fuse these observations through an estimator to improve the quality of their navigation solution while simultaneously mapping the unknown SOPs' states. While navigating, GNSS signals become unavailable, at which point the AVs continue navigating by aiding their INSs' with the SOP pseudoranges. A distributed approach for INS aiding, which exploits the structure of the INS error state transition matrix, is presented and studied over lossy communication channels. This approach does not require transmitting IMU data and allows each AV to maintain cross correlations. The performance is studied in terms of the number of vehicles in the environment and the reliability of the communication channel. The AVs are assumed to communicate only intermittently with a Bernoulli packet loss model [25].

The remainder of this paper is organized as follows. Section II describes the dynamics model of the SOPs and navigating AVs as well as the receivers' observation model. Section III provides an overview of the centralized collaborative framework and identifies the difficulty of maintaining the cross-correlations in a distributed framework. Section IV introduces a distributed SOP-aided INS framework. Section V presents a performance analysis of the distributed SOP-aided INS framework over varying quantity of AVs and communication channel reliability. Section VI presents experimental results demonstrating multiple AVs navigating with cellular signals using the distributed SOP-aided INS framework. Concluding remarks are given in Section VII.

II. MODEL DESCRIPTION

A. SOP Dynamics Model

Each SOP will be assumed to emanate from a spatially-stationary terrestrial transmitter, and its state vector will consist of its 3-D position states $\boldsymbol{r}_{\text{sop}_m} \triangleq \left[x_{\text{sop}_m},\, y_{\text{sop}_m},\, z_{\text{sop}_m}\right]^{\mathsf{T}}$ and clock error states $\boldsymbol{x}_{\text{clk,sop}_m} \triangleq \left[c\delta t_{\text{sop}_m},\, c\dot{\delta t}_{\text{sop}_m}\right]^{\mathsf{T}}$, where c is the speed of light, δt_{sop_m} is the clock bias, $\dot{\delta t}_{\text{sop}_m}$ is the clock drift, $m = 1, \ldots, M$, and M is the total number of SOPs.

The SOP's discretized dynamics are given by

$$\boldsymbol{x}_{\text{sop}_m}(k+1) = \mathbf{F}_{\text{sop}}\, \boldsymbol{x}_{\text{sop}_m}(k) + \boldsymbol{w}_{\text{sop}_m}(k), \quad k = 1, 2, \ldots, \tag{1}$$

where $\boldsymbol{x}_{\text{sop}_m} = \left[\boldsymbol{r}_{\text{sop}_m}^{\mathsf{T}}, \boldsymbol{x}_{\text{clk,sop}_m}^{\mathsf{T}}\right]^{\mathsf{T}}$, $\mathbf{F}_{\text{sop}} = \text{diag}\left[\mathbf{I}_{3\times3}, \mathbf{F}_{\text{clk}}\right]$, $\boldsymbol{w}_{\text{sop}_m}$ is the process noise, which is modeled as a discrete-time (DT) zero-mean white noise sequence with covariance $\mathbf{Q}_{\text{sop}_m} = \text{diag}\left[\mathbf{0}_{3\times3}, c^2\mathbf{Q}_{\text{clk,sop}_m}\right]$, and

$$\mathbf{F}_{\text{clk}} = \begin{bmatrix} 1 & T \\ 0 & 1 \end{bmatrix}, \quad \mathbf{Q}_{\text{clk,sop}_m} = \begin{bmatrix} S_{w_{\delta t_{\text{sop},m}}} T + S_{w_{\dot{\delta} t_{\text{sop},m}}} \frac{T^3}{3} & S_{w_{\dot{\delta} t_{\text{sop},m}}} \frac{T^2}{2} \\ S_{w_{\dot{\delta} t_{\text{sop},m}}} \frac{T^2}{2} & S_{w_{\dot{\delta} t_{\text{sop},m}}} T \end{bmatrix},$$

where T is the constant sampling interval. The terms $S_{w_{\delta t_{\text{sop},m}}}$ and $S_{w_{\dot{\delta} t_{\text{sop},m}}}$ are the clock bias and drift process noise power spectra, respectively, which can be related to the power-law coefficients, $\left\{h_{\alpha,\text{sop}_m}\right\}_{\alpha=-2}^{2}$, which have been shown through laboratory experiments to characterize the power spectral density of the fractional frequency deviation of an oscillator from nominal frequency according to $S_{w_{\delta t_{\text{sop},m}}} \approx \frac{h_{0,\text{sop}_m}}{2}$ and $S_{w_{\dot{\delta} t_{\text{sop},m}}} \approx 2\pi^2 h_{-2,\text{sop}_m}$ [26].

B. Vehicle Dynamics Model

The nth AV-mounted navigating receiver's state vector $\boldsymbol{x}_{r_n}$ is comprised of the INS states $\boldsymbol{x}_{B_n}$ and the receiver's clock error states $\boldsymbol{x}_{\text{clk},r_n} \triangleq \left[c\delta t_{r_n}, c\dot{\delta} t_{r_n}\right]^{\mathsf{T}}$, i.e., $\boldsymbol{x}_{r_n} = \left[\boldsymbol{x}_{B_n}^{\mathsf{T}}, \boldsymbol{x}_{\text{clk},r_n}^{\mathsf{T}}\right]^{\mathsf{T}}$, where $n = 1, \ldots, N$, and N is the total number of AVs.

The INS 16-state vector is

$$\boldsymbol{x}_{B_n} = \left[{}^{B}_{G}\bar{\boldsymbol{q}}_n^{\mathsf{T}}, \quad \boldsymbol{r}_{r_n}^{\mathsf{T}}, \quad \boldsymbol{v}_{r_n}^{\mathsf{T}}, \quad \boldsymbol{b}_{g_n}^{\mathsf{T}}, \quad \boldsymbol{b}_{a_n}^{\mathsf{T}}\right]^{\mathsf{T}},$$

where ${}^{B}_{G}\bar{\boldsymbol{q}}_n$ is the 4-D unit quaternion in vector-scalar form which represents the orientation of the body frame with respect to a global frame [27], e.g., the Earth-centered inertial (ECI) frame; $\boldsymbol{r}_{r_n}$ and $\boldsymbol{v}_{r_n}$ are the 3-D position and velocity, respectively, of the AV's body frame expressed in a global frame; and $\boldsymbol{b}_{g_n}$ and $\boldsymbol{b}_{a_n}$ are the gyroscope and accelerometer biases, respectively.

B.1 Receiver Clock State Dynamics

The nth AV-mounted receiver's clock error states will evolve in time according to

$$\boldsymbol{x}_{\text{clk},r_n}(k+1) = \mathbf{F}_{\text{clk}}\boldsymbol{x}_{\text{clk},r_n}(k) + \boldsymbol{w}_{\text{clk},r_n}(k), \tag{2}$$

where $\boldsymbol{w}_{\text{clk},r_n}$ is the process noise vector, which is modeled as a DT zero-mean white noise sequence with covariance $\mathbf{Q}_{\text{clk},r_n}$, which has an identical form to $\mathbf{Q}_{\text{clk,sop}_m}$, except that $S_{w_{\delta t_{\text{sop},m}}}$ and $S_{w_{\dot{\delta} t_{\text{sop},m}}}$ are now replaced with receiver-specific spectra $S_{w_{\delta t_{r,n}}}$ and $S_{w_{\dot{\delta} t_{r,n}}}$, respectively.

B.2 INS State Dynamics

The IMU on the nth AV contains a triad-gyroscope and a triad-accelerometer which produce measurements $\boldsymbol{z}_{\text{imu}_n} \triangleq \left[\boldsymbol{\omega}_{\text{imu}_n}^{\mathsf{T}}, \boldsymbol{a}_{\text{imu}_n}^{\mathsf{T}}\right]^{\mathsf{T}}$ of the angular rate and specific force, which are modeled as

$$\boldsymbol{\omega}_{\text{imu}_n} = {}^{B}\boldsymbol{\omega}_n + \boldsymbol{b}_{g_n} + \boldsymbol{n}_{g_n} \tag{3}$$

$$\boldsymbol{a}_{\text{imu}_n} = \mathbf{R}\left[{}^{B_k}_{G}\bar{\boldsymbol{q}}_n\right]\left({}^{G}\boldsymbol{a}_n - {}^{G}\boldsymbol{g}_n\right) + \boldsymbol{b}_{a_n} + \boldsymbol{n}_{a_n}, \tag{4}$$

where ${}^{B}\boldsymbol{\omega}_n$ is the 3-D rotational rate vector, ${}^{G}\boldsymbol{a}_n$ is the 3-D acceleration of the IMU in the global frame, ${}^{B_k}_{G}\bar{\boldsymbol{q}}_n$ represents the orientation of the body frame in a global frame at time-step k, $\mathbf{R}\left[\bar{\boldsymbol{q}}_n\right]$ is the equivalent rotation matrix of $\bar{\boldsymbol{q}}_n$, ${}^{G}\boldsymbol{g}_n$ is the acceleration due to gravity of the nth AV in the global frame, and $\boldsymbol{n}_{g_n}$ and $\boldsymbol{n}_{a_n}$ are measurement noise vectors, which are modeled as zero-mean white noise sequences with covariances $\sigma_{g_n}^2\mathbf{I}_{3\times3}$ and $\sigma_{a_n}^2\mathbf{I}_{3\times3}$, respectively. It is worth noting that a non-rotating global reference frame is assumed in the above IMU measurement models. For rotating frames, such as the Earth-centered Earth-fixed frame (ECEF), the rotation rate of the Earth and the Coriolis force should also be modeled, as discussed in [28].

The orientation of the INS will evolve in DT according to

$$ {}^{B_{k+1}}_{G}\bar{\boldsymbol{q}}_n = {}^{B_{k+1}}_{B_k}\bar{\boldsymbol{q}}_n \otimes {}^{B_k}_{G}\bar{\boldsymbol{q}}_n, \tag{5} $$

where ${}^{B_{k+1}}_{B_k}\bar{\boldsymbol{q}}_n$ represents the relative rotation of the nth AV's body frame from time-step k to $k+1$ and $\otimes$ is the quaternion multiplication operator. The unit quaternion ${}^{B_{k+1}}_{B_k}\bar{\boldsymbol{q}}_n$ is the solution to the differential equation

$$ {}^{B_t}_{B_k}\dot{\bar{\boldsymbol{q}}}_n = \frac{1}{2}\boldsymbol{\Omega}\left[{}^{B}\boldsymbol{\omega}_n(t)\right] {}^{B_t}_{B_k}\bar{\boldsymbol{q}}_n, \quad t \in [t_k, t_{k+1}], \tag{6} $$

where $t_k \triangleq kT$ and for any vector $\boldsymbol{\omega} \in \mathbb{R}^3$, the matrix $\boldsymbol{\Omega}[\boldsymbol{\omega}]$ is defined as

$$ \boldsymbol{\Omega}[\boldsymbol{\omega}] \triangleq \begin{bmatrix} -\lfloor \boldsymbol{\omega}\times \rfloor & \boldsymbol{\omega} \\ -\boldsymbol{\omega}^{\mathsf{T}} & 0 \end{bmatrix}, \quad \lfloor \boldsymbol{\omega}\times \rfloor \triangleq \begin{bmatrix} 0 & \omega_3 & -\omega_2 \\ -\omega_3 & 0 & \omega_1 \\ \omega_2 & -\omega_1 & 0 \end{bmatrix}, $$

where ω_i are the elements of the vector $\boldsymbol{\omega}$.

The velocity evolves in time according to

$$ \boldsymbol{v}_{r_n}(k+1) = \boldsymbol{v}_{r_n}(k) + \int_{t_k}^{t_{k+1}} {}^{G}\boldsymbol{a}_n(\tau)d\tau. \tag{7} $$

The position evolves in time according to

$$ \boldsymbol{r}_{r_n}(k+1) = \boldsymbol{r}_{r_n}(k) + \int_{t_k}^{t_{k+1}} \boldsymbol{v}_{r_n}(\tau)d\tau. \tag{8} $$

The evolution of $\boldsymbol{b}_{g_n}$ and $\boldsymbol{b}_{a_n}$ will be modeled as random walk processes, i.e., $\dot{\boldsymbol{b}}_{a_n} = \boldsymbol{w}_{a_n}$ and $\dot{\boldsymbol{b}}_{g_n} = \boldsymbol{w}_{g_n}$ with $\mathbb{E}[\boldsymbol{w}_{g_n}] = \mathbb{E}[\boldsymbol{w}_{a_n}] = \boldsymbol{0}$, $\text{cov}[\boldsymbol{w}_{g_n}] = \sigma^2_{w_{g_n}}\mathbf{I}_3$, and $\text{cov}[\boldsymbol{w}_{a_n}] = \sigma^2_{w_{a_n}}\mathbf{I}_3$. The above attitude, position, and velocity models are discussed in detail in [29].

C. Receiver Observation Model

The pseudorange observation made by the nth receiver on the mth SOP at time-step j, after discretization and mild approximations discussed in [23], is related to the receiver's and SOP's states by

$$ z_{r_n,\text{sop}_m}(j) = \|\boldsymbol{r}_{r_n}(j) - \boldsymbol{r}_{\text{sop}_m}\|_2 + c \cdot \left[\delta t_{r_n}(j) - \delta t_{\text{sop}_m}(j)\right] + v_{r_n,\text{sop}_m}(j), \tag{9} $$

where v_{r_n,sop_m} is modeled as a DT zero-mean white Gaussian sequence with variance $\sigma^2_{r_n,\text{sop}_m}$. The pseudorange observation made by the nth receiver on the lth GNSS SV, after compensating for ionospheric and tropospheric delays is related to the receiver states by

$$ z_{r_n,\text{sv}_l}(j) = \|\boldsymbol{r}_{r_n}(j) - \boldsymbol{r}_{\text{sv}_l}(j)\|_2 + c \cdot [\delta t_{r_n}(j) - \delta t_{\text{sv}_l}(j)] + v_{r_n,\text{sv}_l}(j), \tag{10} $$

where, $z_{r_n,\text{sv}_l} \triangleq z'_{r_n,\text{sv}_l} - c\delta t_{\text{iono}} - c\delta t_{\text{tropo}}$, δt_{iono} and δt_{tropo} are the ionospheric and tropospheric delays, respectively; z'_{r_n,sv_l} is the uncorrected pseudorange; v_{r_n,sv_l} is modeled as a DT zero-mean white Gaussian sequence with variance $\sigma^2_{r_n,\text{sv}_l}$; $l = 1, \ldots, L$; and L is the total number of GNSS SVs.

III. CENTRALIZED COLLABORATIVE SOP-AIDED INERTIAL NAVIGATION OVERVIEW

In this section, an overview the centralized collaborative SOP-aided INS framework that was presented in detail in [7] is provided and the difficulty in moving from a centralized to a distributed framework is discussed.

A. Centralized Framework

Consider N navigating AVs, each of which is equipped with an IMU and receivers that are capable of producing pseudoranges to the same L GNSS SVs and M unknown SOPs. The purpose of the collaborative SOP-aided INS framework is to (i) exploit SOPs to supplement a GNSS-aided INS to improve the accuracy of each AV's navigation solution, (ii) use SOP pseudoranges exclusively as an aiding source to correct the accumulating errors of their INSs when GNSS pseudoranges become unavailable, and (iii) fuse IMU data, GNSS and SOP pseudoranges, and state estimates of all collaborating AVs through an extended Kalman filter (EKF)-based central fusion center (CFC) to improve the estimation performance compared to a single AV using an SOP-aided INS [5].

To exploit SOPs for navigation, their states must be known [30, 31]. However, in many practical scenarios, the SOP transmitter positions are unknown. Furthermore, the SOPs' clock states are dynamic and stochastic; therefore, they must be continuously estimated. To tackle these problems, in addition to estimating the AVs' states, the states of all available SOPs are simultaneously estimated in a radio collaborative SLAM framework. Specifically, the central estimator produces an estimate $\hat{\boldsymbol{x}}(k|j) \triangleq \mathbb{E}[\boldsymbol{x}(k)|\boldsymbol{Z}^j]$ of $\boldsymbol{x}(k)$ and an associated estimation error covariance $\mathbf{P}(k|j) \triangleq \mathbb{E}[\tilde{\boldsymbol{x}}(k|j)\tilde{\boldsymbol{x}}^\mathsf{T}(k|j)|\boldsymbol{Z}^j]$ where

$$\boldsymbol{x} \triangleq \left[\boldsymbol{x}_{r_1}^\mathsf{T}, \ldots, \boldsymbol{x}_{r_N}^\mathsf{T}, \boldsymbol{x}_{\mathrm{sop}_1}^\mathsf{T}, \ldots, \boldsymbol{x}_{\mathrm{sop}_M}^\mathsf{T}\right]^\mathsf{T}, \ \boldsymbol{z} \triangleq \left[\boldsymbol{z}_{\mathrm{sv}}^\mathsf{T}, \boldsymbol{z}_{\mathrm{sop}}^\mathsf{T}\right]^\mathsf{T},$$

$$\boldsymbol{z}_{\mathrm{sv}} \triangleq \left[\boldsymbol{z}_{r_1,\mathrm{sv}}^\mathsf{T}, \ldots, \boldsymbol{z}_{r_N,\mathrm{sv}}^\mathsf{T}\right]^\mathsf{T}, \quad \boldsymbol{z}_{\mathrm{sop}} \triangleq \left[\boldsymbol{z}_{r_1,\mathrm{sop}}^\mathsf{T}, \ldots, \boldsymbol{z}_{r_N,\mathrm{sop}}^\mathsf{T}\right]^\mathsf{T},$$

$$\boldsymbol{z}_{r_n,\mathrm{sv}} = \left[z_{r_n,\mathrm{sv}_1}, \ldots, z_{r_n,\mathrm{sv}_L}\right]^\mathsf{T}, \ \boldsymbol{z}_{r_n,\mathrm{sop}} = \left[z_{r_n,\mathrm{sop}_1}, \ldots, z_{r_n,\mathrm{sop}_M}\right]^\mathsf{T},$$

where $k \geq j$, j is the last time-step an INS-aiding source was available, and $\boldsymbol{Z}^j \triangleq \{\boldsymbol{z}(i)\}_{i=1}^j$. A high-level diagram of this framework is illustrated in Fig. 1.

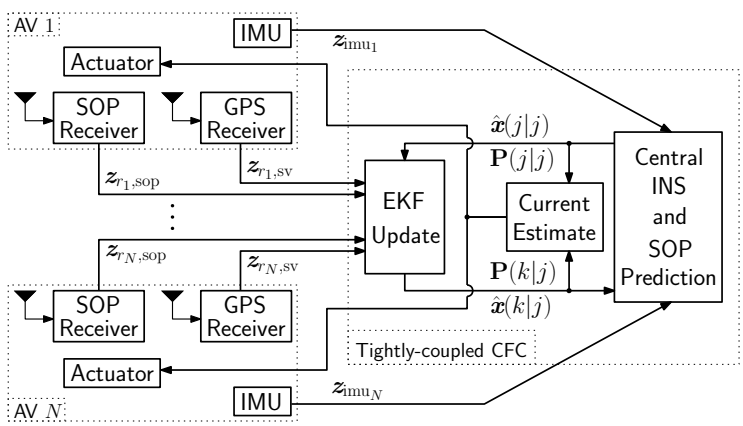

Fig. 1. Centralized collaborative SOP-aided INS. All N collaborating AVs send their IMU data $\boldsymbol{z}_{\mathrm{imu}_n}$, GNSS pseudoranges $\boldsymbol{z}_{r_n,\mathrm{sv}}$, and SOP pseudoranges $\boldsymbol{z}_{r_n,\mathrm{sop}}$ to a tightly-coupled EKF-based CFC, which produces a state estimate $\hat{\boldsymbol{x}}$ and a corresponding estimation error covariance $\mathbf{P}$.

B. Centralized State and Covariance Prediction

Between EKF updates, which take place when either GPS or SOP pseudorange become available, the central estimator uses IMU data transmitted from all AVs and the clock model described in Section II to propagate the state estimate from $\hat{\boldsymbol{x}}(j|j)$ to $\hat{\boldsymbol{x}}(k|j)$ and produce a corresponding prediction error covariance $\mathbf{P}(k|j)$. Assuming there are $K = k - j$ steps between EKF updates, the K-step prediction can be shown to be given by

$$\mathbf{P}(k|j) = \mathbf{F}(k,j)\mathbf{P}(j|j)\mathbf{F}^\mathsf{T}(k,j) + \bar{\mathbf{Q}}(k,j), \tag{11}$$

$$\mathbf{F}(k,j) \triangleq \mathrm{diag}\left[\mathbf{F}_{r_1}(k,j), \ldots, \mathbf{F}_{r_N}(k,j), \mathbf{F}_{\mathrm{sop}}^K, \ldots, \mathbf{F}_{\mathrm{sop}}^K\right],$$

$$\bar{\mathbf{Q}}(k,j) \triangleq \mathrm{diag}\left[\bar{\mathbf{Q}}_{r_1}(k,j), \ldots, \bar{\mathbf{Q}}_{r_N}(k,j), \bar{\mathbf{Q}}_{\mathrm{sop}_1}(k,j), \ldots, \bar{\mathbf{Q}}_{\mathrm{sop}_M}(k,j)\right],$$

where $\mathbf{F}_{r_n}(k,j)$ is the nth AV's DT error state-transition matrix from time-step j to time-step k and

$$\bar{\mathbf{Q}}_{r_n}(k,j) \triangleq \sum_{i=j}^{k} \mathbf{F}_{r_n}(i,j)\mathbf{Q}_{r_n}(i)\mathbf{F}_{r_n}^{\mathsf{T}}(i,j), \quad \bar{\mathbf{Q}}_{\text{sop}_m}(k,j) \triangleq \sum_{i=j}^{k} \mathbf{F}_{\text{sop}}^{(i-j)}\mathbf{Q}_{\text{sop}_m}[\mathbf{F}_{\text{sop}}^{\mathsf{T}}]^{(i-j)},$$

$$\mathbf{F}_{\text{sop}}^{\kappa} = \begin{cases} \prod_{l=1}^{\kappa} \mathbf{F}_{\text{sop}} & \kappa > 0, \\ \mathbf{I}_{5\times 5} & \kappa = 0, \end{cases}$$

and $\mathbf{Q}_{r_n}(i) \triangleq \text{diag}\left[\mathbf{Q}_{\text{d},B_n}(i),\, c^2\mathbf{Q}_{\text{clk},r_n}\right]$, where $\mathbf{Q}_{\text{d},B_n}$ is the nth AV's DT linearized INS state process noise covariance. The detailed derivations and the structure of $\mathbf{Q}_{\text{d},B_n}$ are described in [28,32].

To analyze the structure of (11) after the prediction, consider the partitioned form

$$\mathbf{P}(k|j) = \begin{bmatrix} \mathbf{P}_r(k|j) & \mathbf{P}_{r,\text{sop}}(k|j) \\ \mathbf{P}_{r,\text{sop}}^{\mathsf{T}}(k|j) & \mathbf{P}_{\text{sop}}(k|j) \end{bmatrix},$$

where $\mathbf{P}_r$ is the covariance associated with all the AVs' states, $\mathbf{P}_{\text{sop}}$ is the covariance associated with all the sops' states, and $\mathbf{P}_{r,\text{sop}}$ is their cross-covariance. The prediction of $\mathbf{P}_r$ has the form

$$\mathbf{P}_r(k|j) = \begin{bmatrix} \mathbf{F}_{r_1}(k,j)\mathbf{P}_{r_1}(j|j)\mathbf{F}_{r_1}^{\mathsf{T}}(k,j)+\bar{\mathbf{Q}}_{r_1}(k,j) & \mathbf{F}_{r_1}(k,j)\mathbf{P}_{r_2}(j|j)\mathbf{F}_{r_2}^{\mathsf{T}}(k,j) & \cdots \\ \mathbf{F}_{r_2}(k,j)\mathbf{P}_{r_2}(j|j)\mathbf{F}_{r_1}^{\mathsf{T}}(k,j) & \mathbf{F}_{r_2}(k,j)\mathbf{P}_{r_2}(j|j)\mathbf{F}_{r_2}^{\mathsf{T}}(k,j)+\bar{\mathbf{Q}}_{r_2}(k,j) & \\ \vdots & & \ddots \end{bmatrix}, \tag{12}$$

where $\mathbf{F}_{r_n}(k,j) \triangleq \text{diag}\left[\mathbf{\Phi}_{B_n}(k,j),\, \mathbf{F}_{\text{clk}}^{K}\right]$ and $\mathbf{\Phi}_{B_n}$ is the nth AV's DT linearized INS state transition matrix, which has the structure

$$\mathbf{\Phi}_{B_n}(k,j) = \begin{bmatrix} \mathbf{I}_{3\times 3} & \mathbf{0}_{3\times 3} & \mathbf{0}_{3\times 3} & \mathbf{\Phi}_{\boldsymbol{qb}_{g_n}}(k,j) & \mathbf{\Phi}_{\boldsymbol{qb}_{a_n}}(k,j) \\ \mathbf{\Phi}_{\boldsymbol{pq}_n}(k,j) & \mathbf{I}_{3\times 3} & \mathbf{I}_{3\times 3}T & \mathbf{\Phi}_{\boldsymbol{pb}_{g_n}}(k,j) & \mathbf{\Phi}_{\boldsymbol{pb}_{a_n}}(k,j) \\ \mathbf{\Phi}_{\boldsymbol{vq}_n}(k,j) & \mathbf{0}_{3\times 3} & \mathbf{I}_{3\times 3} & \mathbf{\Phi}_{\boldsymbol{vb}_{g_n}}(k,j) & \mathbf{\Phi}_{\boldsymbol{vb}_{a_n}}(k,j) \\ \mathbf{0}_{3\times 3} & \mathbf{0}_{3\times 3} & \mathbf{0}_{3\times 3} & \mathbf{I}_{3\times 3} & \mathbf{0}_{3\times 3} \\ \mathbf{0}_{3\times 3} & \mathbf{0}_{3\times 3} & \mathbf{0}_{3\times 3} & \mathbf{0}_{3\times 3} & \mathbf{I}_{3\times 3} \end{bmatrix},$$

where the blocks $\mathbf{\Phi}_{\boldsymbol{qb}_{g_n}}, \mathbf{\Phi}_{\boldsymbol{qb}_{a_n}}, \mathbf{\Phi}_{\boldsymbol{pq}_n}, \mathbf{\Phi}_{\boldsymbol{pb}_{g_n}}, \mathbf{\Phi}_{\boldsymbol{pb}_{a_n}}, \mathbf{\Phi}_{\boldsymbol{vq}_n}, \mathbf{\Phi}_{\boldsymbol{vb}_{g_n}}$, and $\mathbf{\Phi}_{\boldsymbol{vb}_{a_n}}$ are 3×3 matrices whose elements depend on the IMU data from AV n. The challenge in moving from a centralized to a distributed aided INS is revealed in the structure of (12). Specifically, the propagation of the cross-covariance term between any two vehicles n and n' requires both $\mathbf{\Phi}_{B_n}$ and $\mathbf{\Phi}_{B_{n'}}$, which are dependent on the respective vehicle's IMU data between time t_k and t_j. In a central estimator, under a perfect communication channel assumption, this is not an issue since the prediction (12) is readily calculated using IMU data reliably transmitted from each AV to a CFC. However, this approach may be impractical due to several reasons: (1) transmitting all IMU data requires a large communication bandwidth, (2) real communication channels are imperfect (lossy), and (3) access to the raw IMU data may not be available. Motivated by these concerns, a distributed approach that can compute (12) with minimal communication between AVs is desired.

IV. DISTRIBUTED SOP-AIDED INERTIAL NAVIGATION

In this section, the distributed framework depicted in Fig. 2 is described. Each AV employs its own EKF that maintains the global estimate $\hat{\boldsymbol{x}}$ (maintained in the Aiding correction block). Instead of transmitting IMU data to a central estimator, each AV, uses its own local IMU data $\boldsymbol{z}_{\text{imu}_\text{n}}$ between t_j to t_k to propagate $\hat{\boldsymbol{x}}(j|j)$ to $\hat{\boldsymbol{x}}(k|j)$ and produce $\mathbf{\Phi}_{B_n}(k,j)$. When a set of pseudoranges becomes available, each vehicle broadcasts a packet:

$$\mathbf{\Lambda}_n(k) \triangleq \left\{\hat{\boldsymbol{x}}_{B_n}(k|j), \mathbf{\Phi}_{B_n}(k,j), \boldsymbol{z}_{r_n,\text{sv}}(k), \boldsymbol{z}_{r_n,\text{sop}}(k)\right\}. \tag{13}$$

Note that the state predictions $\left\{\hat{\boldsymbol{x}}_{\text{clk}_{r_n}}(k|j)\right\}_{n=1}^{N}$ and $\left\{\hat{\boldsymbol{x}}_{\text{sop}}(k|j)\right\}_{m=1}^{M}$ are not transmitted, since their dynamics (2) and (1) are linear time-invariant; therefore, the predictions can be performed at each vehicle. Assuming a fully connected graph, i.e., all AVs can send and receive packets to all AVs as depicted in Fig. 2, this framework will perform equivalently to the centralized framework depicted in Fig. 1 for the following reasons: (i) the global propagation

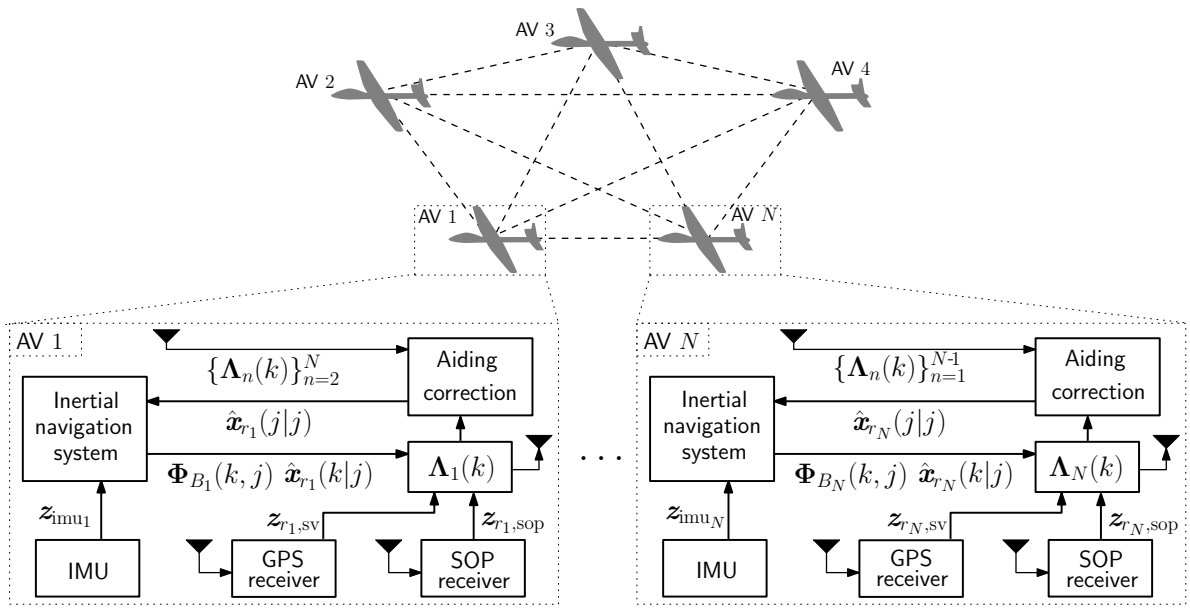

Fig. 2. Distributed SOP-aided INS framework with a fully connected graph.

(12) can be performed at each vehicle, (ii) each vehicle has access to all $\{\hat{\boldsymbol{x}}_{r_n}(k|j)\}_{n=1}^{N}$, which are necessary for the computation of the measurement Jacobians, and (iii) each vehicle has access to all measurements. For these reasons, each AV can perform the global centralized update. However, the transmission of $\mathbf{\Phi}_{B_n}$ is costly, since it is a 15×15 matrix, which requires the transmission of 225 elements every update. Nevertheless, by exploiting the sparsity of $\mathbf{\Phi}_{B_n}$, one can reduce the transmitted elements to 72.

V. PERFORMANCE CHARACTERIZATION

A. Channel Loss Model

The successful arrival of the data packets $\{\mathbf{\Lambda}_n(k)\}_{n=1}^{N}$ will be governed by a Bernoulli independent and identically distributed sequence. This can be shown to modify the measurement update to take the form

$$\begin{aligned}\hat{\boldsymbol{x}}(k|k) &= \boldsymbol{x}(k|j) + \gamma(k)\mathbf{K}(k)\left[\boldsymbol{z}(k) - \hat{\boldsymbol{z}}(k)\right],\\ \mathbf{P}(k|k) &= \mathbf{P}(k|j) - \gamma(k)\mathbf{K}(k)\mathbf{H}(k)\mathbf{P}(k|j),\end{aligned}$$

where

$$\gamma(k) \sim \mathcal{B}(1-p) = \begin{cases} p & \gamma(k) = 0 \\ 1-p & \gamma(k) = 1, \end{cases}$$

where $\mathbf{K}$ is the Kalman gain matrix, $\hat{\boldsymbol{z}}$ is the predicted measurement, $\mathbf{H}$ is the measurement Jacobian evaluated at the state prediction $\hat{\boldsymbol{x}}(k|j)$, and γ is a Bernoulli random variable with probability of failure p [33]. Immediately following the update, k is set to j ($k \equiv j$). The structures of $\mathbf{H}$ and $\mathbf{K}$ are dependent on how the pseudoranges are fused in the estimator, e.g., as time-of-arrival (TOA) or time-difference-of-arrival (TDOA), and are described in detail in [7]. Note that if communication of the data packets $\{\mathbf{\Lambda}_n(k)\}_{n=1}^{N}$ fail ($\gamma(k) = 0$), the updated state and covariance is simply set to the predicted values $\boldsymbol{x}(k|j)$ and $\mathbf{P}(k|j)$, respectively. Subsequently, k is set to j and the estimator returns to the prediction (11).

B. Simulation Settings and Results

An environment comprising six SOPs and $N = 4$ AVs were simulated. The clock states for each AV-mounted receiver was simulated according to (2), with $\{h_{0,r_n}, h_{-2,r_n}\}_{n=1}^{4} = \{9.4 \times 10^{-20}, 3.8 \times 10^{-21}\}$, which corresponds to a typical

temperature-compensated crystal oscillator (TCXO). Each simulated trajectory corresponded to an unmanned aerial vehicle (UAV), whose trajectories were generated using a standard six degree-of-freedom (6DoF) kinematic model of airplanes [28].

IMU data from a triad gyroscope and a triad accelerometer were generated at 100 Hz according to (3) and (4), respectively. The magnitude of the bias errors and their driving statistics are determined by the grade of the IMU. Data for a consumer-grade IMU was generated for this work.

GPS L1 C/A pseudoranges were generated at 1 Hz according to (10) using SV orbits produced from Receiver Independent Exchange (RINEX) files downloaded on May 31, 2017 from a Continuously Operating Reference Station (CORS) server [34]. The GPS signals were set to be available for $t \in [0, 50)$ seconds, and unavailable for $t \in [50, 170]$ seconds. Pseudoranges were generated to six SOPs at 5 Hz according to (9) and the SOP dynamics discussed in Subsection II-A. Each SOP was set to be equipped with a typical oven-controlled crystal oscillator (OCXO), with $\{h_{0,\text{sop}_m}, h_{-2,\text{sop}_m}\} = \{8 \times 10^{-20}, 4 \times 10^{-23}\}$, where $m = 1, ..., 6$. The SOP emitter positions $\{\boldsymbol{r}_{\text{sop}_m}\}_{m=1}^{6}$ were surveyed from cellular tower locations in Portland, Oregon. The simulated trajectories, SOP positions, and the vehicles' positions at the time GPS was set to become unavailable are illustrated in Fig. 3. To avoid cluttering the figure, the trajectories of AV 3 and AV 4 are not shown; however, their trajectory profiles are identical to AV 1 and AV 2, respectively, their initial positions started towards the bottom left and right of the figure, respectively, and their initial heading was towards the center of the figure.

Three runs were simulated. In the first two runs, the distributed SOP-aided INS was employed in an environment with a probability of packet loss set to $p = 0$ and $p = 0.7$, respectively. The resulting position and orientation estimation errors and corresponding 3σ bounds are plotted in Fig. 4 for using (i) the centralized framework described in Section III and (ii) the distributed framework discussed in Section IV. The third run employs a traditional GPS-aided INS for a comparative analysis.

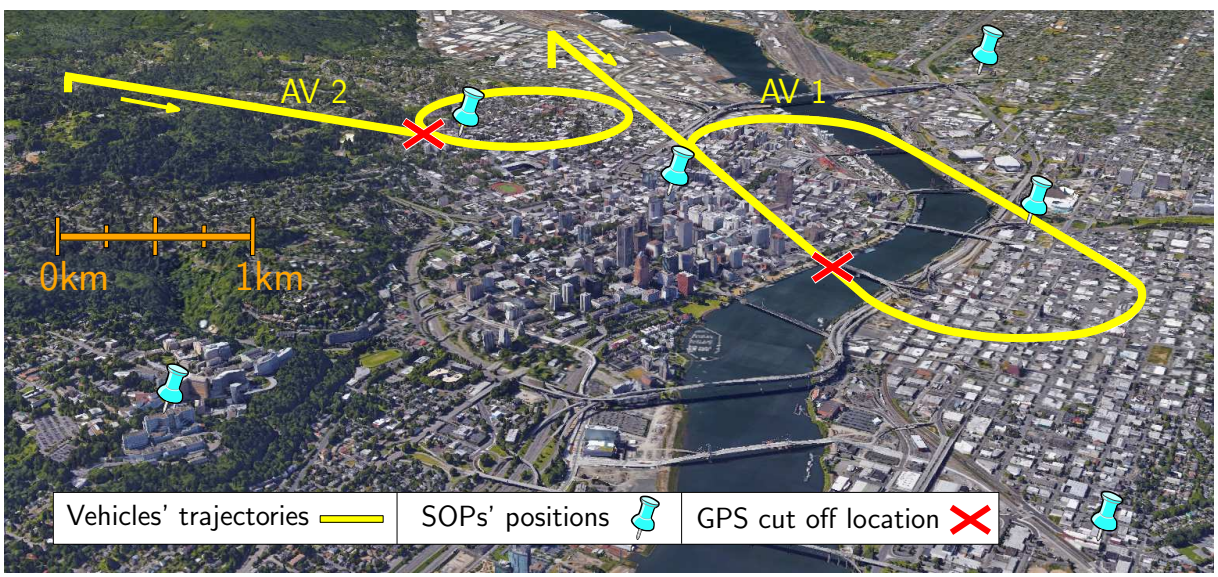

Fig. 3. True UAVs' traversed trajectories (yellow), SOP locations (blue pins), and the vehicles' positions at the time GPS was cut off (red).

The following may be concluded from these plots. First, note that the distributed trajectories (black for $p = 0$ and blue for $p = 7$) are coincident with the centralized trajectories. Second, even with $p = 0.7$, the estimation errors produce by the distributed SOP-aided INS appear to be bounded after GPS cut-off. To further investigate the affect of the probability of packet loss p, 60 simulations were conducted. The probability of loss was swept over $p \in [0, 0.9]$ with increments of $\Delta p = 0.1$. For each p, N was varied from $N = 2, \ldots, 6$. The resulting 3-D root mean squared error (RMSE) time histories of AV 1, $\text{RMSE}(k) = \sqrt{\text{tr}[\mathbf{P}_{r_1}(k)]}$, is plotted in Fig. 5 and the final RMSE versus p and N is plotted in Fig. 6. Similar figures were noted for the other AVs.

The plots in Fig. 5 indicate that even with a probability of packet drop as large as $p = 0.9$, the errors reduce when a measurement update is processed. The error growth due to the increase in p can be compensated for partially by deploying additional collaborating AVs into the environment. This relationship is made more clear in the final RMSE surface plot in Fig. 6. The black grid represents the final RMSE of a single AV navigating with an SOP-aided INS, which inherently has $p = 0$. The points on the surface below the grid can be used to determine how many AVs are required in an environment with a probability of packet loss p to perform comparably to a single AV navigating with an SOP-aided INS.

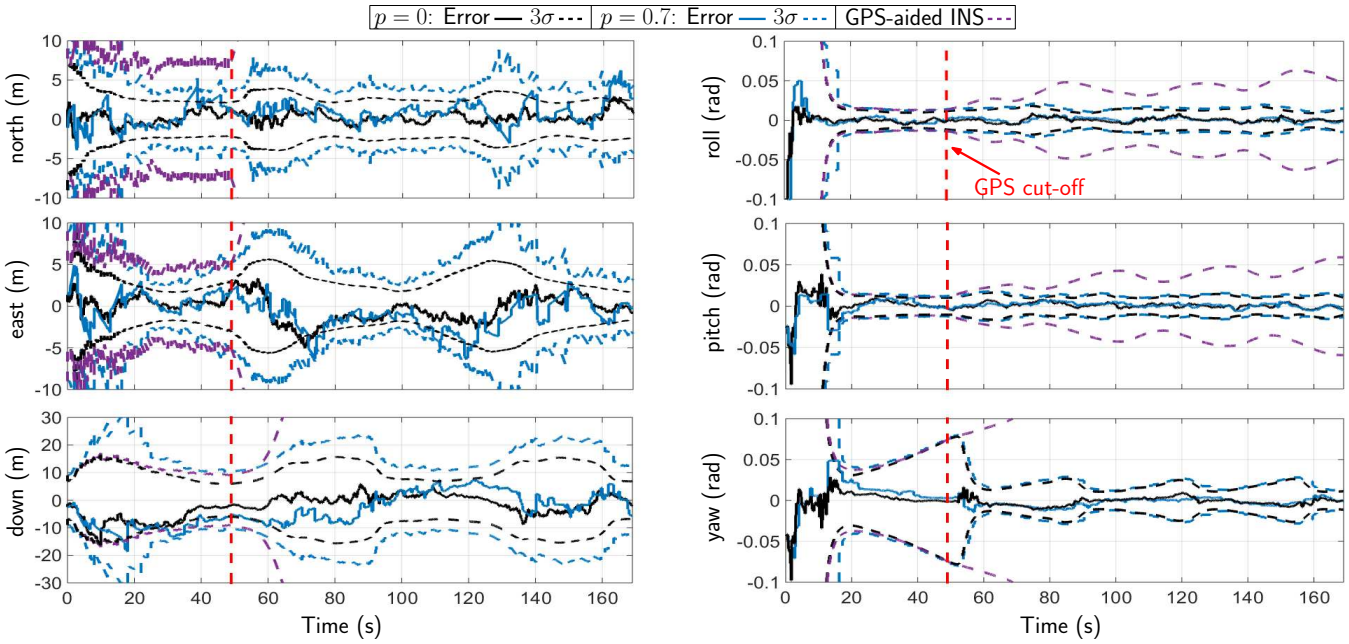

Fig. 4. Position and orientation estimation errors and corresponding 3σ bounds for $N = 4$ AVs and a probability of packet loss p. The black and blue estimation error trajectories correspond $p = 0$ and $p = 0.7$, respectively. The errors produced by the centralized framework are plotted in green for each case.

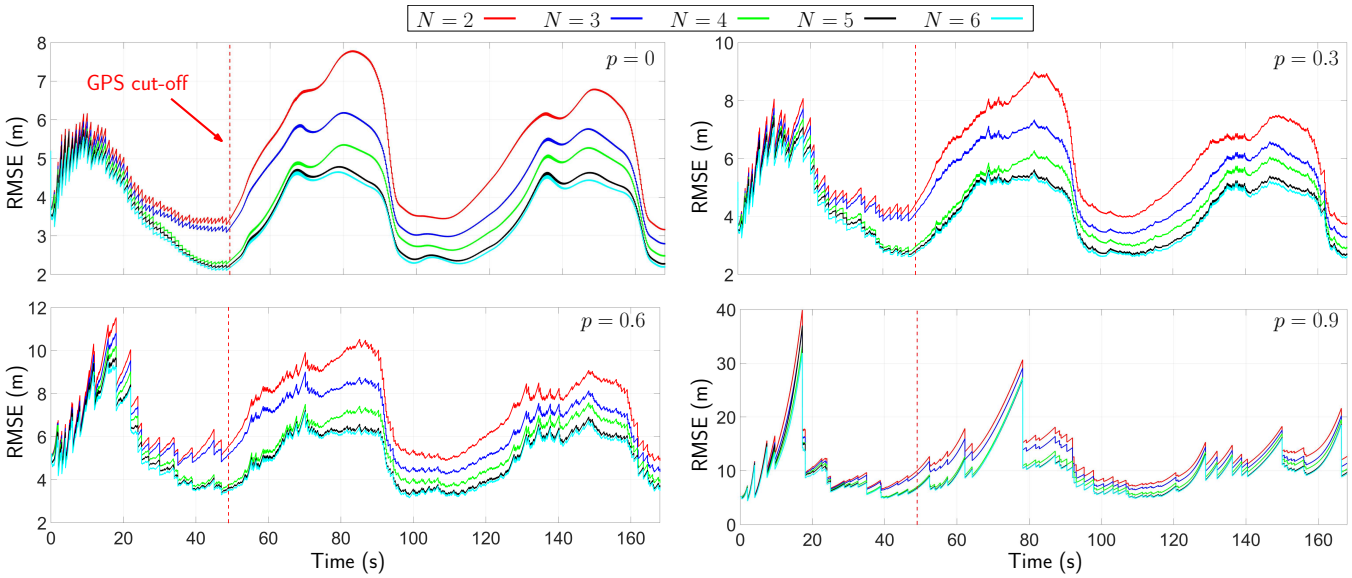

Fig. 5. RMSE time history for a varying number of AVs $N = 2, \ldots, 6$ and probability of packet loss $p = 0, 0.3, 0.6$, and 0.9 for AV 1.

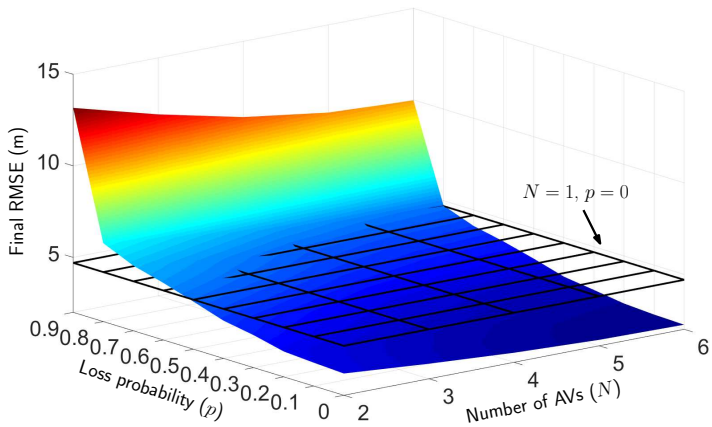

Fig. 6. Final RMSE surface for an AV using a distributed SOP-aided INS after 120 seconds of GPS unavailability in an environment with six SOPs. The number of collaborating AVs was varied from $N = 2, ..., 6$ and the probability of packet loss was varied from $p = 0, ..., 0.9$. Each point on the surface corresponds to one of the AV's final RMSE of its position estimate, given by $\text{RMSE}(k) = \sqrt{\text{tr}[\mathbf{P}_{r_1}(k)]}$. The black grid corresponds to the same AV's final RMSE navigating without collaboration ($p = 0$) using an SOP-aided INS.

VI. EXPERIMENTAL RESULTS

A field experiment was conducted in Riverside, California to demonstrate the performance of the distributed SOP-aided INS framework with intermittent communication. To this end, two unmanned aerial vehicles (UAVs) were each equipped with a two-channel Ettus® universal software radio peripheral (USRP) and a consumer-grade cellular and GPS antenna. Each USRP was tuned to 1575.47 MHz and 883.75 MHz to synchronously sample all available GPS L1 C/A signals and all Verizon cellular base transceiver stations (BTSs) whose signals were modulated through code division multiple access (CDMA). The signals were processed off-line through the Multichannel Adaptive TRansceiver Information eXtractor (MATRIX) SDR, which produced pseudorange observables to all GPS SVs in view and two cellular BTSs [13]. The IMU data was sampled from each UAV's on-board proprietary navigation system, which was developed by Autel Robotics®. Communication between the UAVs was simulated to be intermittent according to a Bernoulli channel model with packet delivery failure probability p. The experimental setup is illustrated in Fig. 7.

The UAVs flew commanded trajectories over a 90 second period in the vicinity of the two BTSs as illustrated in Figs. 8 (a)-(c). Three estimators were implemented to estimate the flown trajectories: (i) the centralized collaborative SOP-aided INS with perfect communication ($p = 0$), as described in Section III, (ii) the distributed SOP-aided INS with intermittent communication ($p = 0.3$), as described in Section IV, and for comparative analysis, (iii) a traditional GPS-aided INS.

Each estimator had access to GPS SV pseudoranges for only the first 75 seconds of the run. The North-East RMSEs of the traditional GPS-aided INSs' navigation solutions after GPS became unavailable were 9.9 and 14.55 meters, respectively. The RMSEs of the UAVs' trajectories for the SOP-aided INS ($p = 0$) were 4.0 and 4.3 meters, respectively, and the final localization error of the cellular BTSs were 25.9 and 11.5 meters, respectively. The RMSEs of the UAVs' trajectories for the SOP-aided INS with intermittent communication ($p = 0.3$) were 8.4 and 4.9 meters, respectively, and the final localization error of the cellular BTSs were 43.5 and 27.8 meters, respectively. The North-East 99th-percentile initial and final uncertainty ellipses of the BTSs position states are illustrated in Fig. 8 (a), (d), and (e). The UAVs' RMSEs and final errors are tabulated in Table I. It is worth noting that this experiment consisted of only two AVs collaborating AVs exploiting two cellular SOP BTSs. It is expected that the increase of the RMSE when p got increased from $p = 0$ to $p = 0.3$ to be less significant when more AVs and SOPs get included.

TABLE I
EXPERIMENTAL ESTIMATION ERRORS

Framework	**Unaided INS**		**SOP-aided INS** ($p = 0$)		($p = 0.3$)	
Vehicle	UAV 1	UAV 2	UAV 1	UAV 2	UAV 1	UAV 2
RMSE (m)	9.9	14.5	4.0	4.3	8.4	4.9
Final error (m)	27.8	24.5	6.3	4.3	14.0	6.1

Fig. 7. Experimental hardware setup.

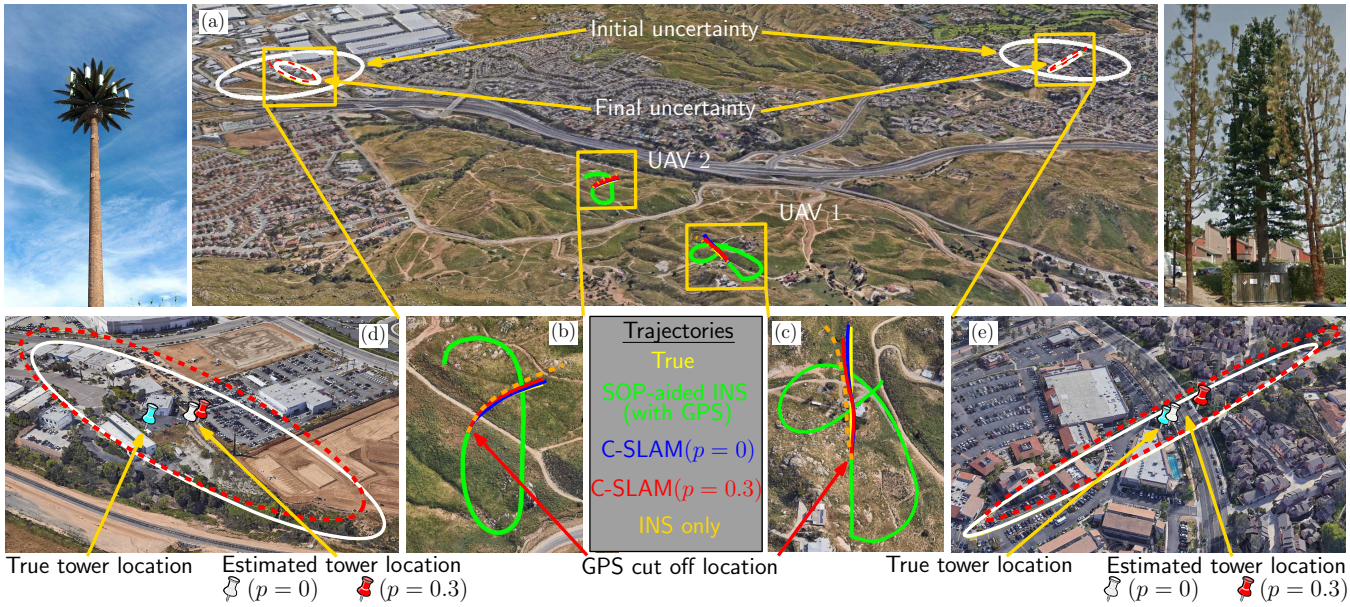

Fig. 8. Experimental results demonstrating two UAVs collaboratively aiding their INSs by exploiting two cellular SOP BTSs with the framework depicted in Fig. 2. The white initial and final BTS position uncertainty ellipses in (a),(d), and (e) correspond to a probability of packet loss $p = 0$, whereas the red correspond to $p = 0.3$. Image: Google Earth.

VII. Conclusions

This work studied a distributed SOP-aided INS framework subject to intermittent communication between AVs. It was shown that a distributed approach performs identically to a centralized framework when all AVs transmit their linearized DT INS state transition matrix along with pseudorange observations on SOPs and state estimates. The performance of the framework was characterized over the probability p of communication failure using a Bernoulli packet loss model and the number of collaborating AVs N. Moreover, experimental results were presented demonstrating two UAVs navigating using two cellular CDMA BTSs in the absence of GPS. The UAVs' trajectory final error reductions were 77.3% and 82.4%, respectively, with perfect communication and 49.6% and 75.1%, respectively, with intermittent communication using $p = 0.3$, when compared to unaided INSs.

Acknowledgment

This work was supported in part by the Office of Naval Research (ONR) under Grant N00014-16-1-2305 and in part by the National Science Foundation (NSF) under Grant 1566240. This work was also supported in part by a grant from the National Center for Sustainable Transportation (NCST), supported by the U.S. Department of Transportation (USDOT) through the University Transportation Centers Program. The authors would like to thank Paul F. Roysdon for his help with data simulation.

References

[1] J. Raquet and R. Martin, "Non-GNSS radio frequency navigation," in *Proceedings of IEEE International Conference on Acoustics, Speech and Signal Processing*, March 2008, pp. 5308–5311.

[2] Z. Kassas, "Analysis and synthesis of collaborative opportunistic navigation systems," Ph.D. dissertation, The University of Texas at Austin, USA, 2014.

[3] Z. Kassas, J. Khalife, K. Shamaei, and J. Morales, "I hear, therefore I know where I am: Compensating for GNSS limitations with cellular signals," *IEEE Signal Processing Magazine*, pp. 111–124, September 2017.

[4] P. MacDoran, M. Mathews, K. Gold, and J. Alvarez, "Multi-sensors, signals of opportunity augmented GPS/GNSS challenged navigation," in *Proceedings of ION International Technical Meeting Conference*, September 2013, pp. 2552–2561.

[5] J. Morales, P. Roysdon, and Z. Kassas, "Signals of opportunity aided inertial navigation," in *Proceedings of ION GNSS Conference*, September 2016, pp. 1492–1501.

[6] Z. Kassas, J. Morales, K. Shamaei, and J. Khalife, "LTE steers UAV," *GPS World Magazine*, vol. 28, no. 4, pp. 18–25, April 2017.

[7] J. Morales, J. Khalife, and Z. Kassas, "Collaborative autonomous vehicles with signals of opportunity aided inertial navigation systems," in *Proceedings of ION International Technical Meeting Conference*, January 2017, 805–818.

[8] A. Soloviev, "Tight coupling of GPS, INS, and laser for urban navigation," *IEEE Transactions on Aerospace and Electronic Systems*, vol. 46, no. 4, pp. 1731–1746, October 2010.

[9] G. Grenon, P. An, S. Smith, and A. Healey, "Enhancement of the inertial navigation system for the morpheus autonomous underwater vehicles," *IEEE Journal of Oceanic Engineering*, vol. 26, no. 4, pp. 548–560, October 2001.

[10] J. McEllroy, "Navigation using signals of opportunity in the AM transmission band," Master's thesis, Air Force Institute of Technology, Wright-Patterson Air Force Base, Ohio, USA, 2006.

[11] V. Moghtadaiee and A. Dempster, "Indoor location fingerprinting using FM radio signals," *IEEE Transactions on Broadcasting*, vol. 60, no. 2, pp. 336–346, June 2014.

[12] C. Yang, T. Nguyen, and E. Blasch, "Mobile positioning via fusion of mixed signals of opportunity," *IEEE Aerospace and Electronic Systems Magazine*, vol. 29, no. 4, pp. 34–46, April 2014.

[13] J. Khalife, K. Shamaei, and Z. Kassas, "A software-defined receiver architecture for cellular CDMA-based navigation," in *Proceedings of IEEE/ION Position, Location, and Navigation Symposium*, April 2016, pp. 816–826.

[14] K. Shamaei, J. Khalife, and Z. Kassas, "Performance characterization of positioning in LTE systems," in *Proceedings of ION GNSS Conference*, September 2016, pp. 2262–2270.

[15] K. Shamaei, J. Khalife, and Z. Kassas, "Comparative results for positioning with secondary synchronization signal versus cell specific reference signal in LTE systems," in *Proceedings of ION International Technical Meeting Conference*, January 2017, pp. 1256–1268.

[16] M. Rabinowitz and J. Spilker, Jr., "A new positioning system using television synchronization signals," *IEEE Transactions on Broadcasting*, vol. 51, no. 1, pp. 51–61, March 2005.

[17] P. Thevenon, S. Damien, O. Julien, C. Macabiau, M. Bousquet, L. Ries, and S. Corazza, "Positioning using mobile TV based on the DVB-SH standard," *NAVIGATION, Journal of the Institute of Navigation*, vol. 58, no. 2, pp. 71–90, 2011.

[18] M. Joerger, L. Gratton, B. Pervan, and C. Cohen, "Analysis of Iridium-augmented GPS for floating carrier phase positioning," *NAVIGATION, Journal of the Institute of Navigation*, vol. 57, no. 2, pp. 137–160, 2010.

[19] K. Pesyna, Z. Kassas, and T. Humphreys, "Constructing a continuous phase time history from TDMA signals for opportunistic navigation," in *Proceedings of IEEE/ION Position Location and Navigation Symposium*, April 2012, pp. 1209–1220.

[20] I. Bisio, M. Cerruti, F. Lavagetto, M. Marchese, M. Pastorino, A. Randazzo, and A. Sciarrone, "A trainingless WiFi fingerprint positioning approach over mobile devices," *IEEE Antennas and Wireless Propagation Letters*, vol. 13, pp. 832–835, 2014.

[21] J. Khalife, Z. Kassas, and S. Saab, "Indoor localization based on floor plans and power maps: Non-line of sight to virtual line of sight," in *Proceedings of ION GNSS Conference*, September 2015, pp. 2291–2300.

[22] H. Durrant-Whyte and T. Bailey, "Simultaneous localization and mapping: part I," *IEEE Robotics & Automation Magazine*, vol. 13, no. 2, pp. 99–110, June 2006.

[23] Z. Kassas and T. Humphreys, "Observability analysis of collaborative opportunistic navigation with pseudorange measurements," *IEEE Transactions on Intelligent Transportation Systems*, vol. 15, no. 1, pp. 260–273, February 2014.

[24] C. Yang and A. Soloviev, "Simultaneous localization and mapping of emitting radio sources-SLAMERS," in *Proceedings of ION GNSS Conference*, September 2015, pp. 2343–2354.

[25] S. Kluge, K. Reif, and M. Brokate, "Stochastic stability of the extended Kalman filter with intermittent observations," *IEEE Transactions on Automatic Control*, vol. 55, no. 2, pp. 514–518, 2010.

[26] A. Thompson, J. Moran, and G. Swenson, *Interferometry and Synthesis in Radio Astronomy*, 2nd ed. John Wiley & Sons, 2001.

[27] N. Trawny and S. Roumeliotis, "Indirect Kalman filter for 3D attitude estimation," University of Minnesota, Dept. of Comp. Sci. & Eng., Tech. Rep. 2005-002, March 2005.

[28] P. Groves, *Principles of* GNSS*, Inertial, and Multisensor Integrated Navigation Systems*, 2nd ed. Artech House, 2013.

[29] M. Shelley, "Monocular visual inertial odometry," Master's thesis, Technical University of Munich, Germany, 2014.

[30] Z. Kassas, V. Ghadiok, and T. Humphreys, "Adaptive estimation of signals of opportunity," in *Proceedings of ION GNSS Conference*, September 2014, pp. 1679–1689.

[31] J. Morales and Z. Kassas, "Optimal receiver placement for collaborative mapping of signals of opportunity," in *Proceedings of ION GNSS Conference*, September 2015, pp. 2362–2368.

[32] J. Farrell and M. Barth, *The Global Positioning System and Inertial Navigation*. New York: McGraw-Hill, 1998.

[33] X. Liu, L. Li, Z. Li, T. Fernando, and H. Iu, "Stochastic stability condition for the extended Kalman filter with intermitent observations," *IEEE Transactions on Circuits and Systems*, vol. 64, no. 3, pp. 334–338, March 2017.

[34] R. Snay and M. Soler, "Continuously operating reference station (CORS): history, applications, and future enhancements," *Journal of Surveying Engineering*, vol. 134, no. 4, pp. 95–104, November 2008.